Protein Science (1999), *8*:2041–2054. Cambridge University Press. Printed in the USA.

Backbone dynamics of the human CC chemokine eotaxin: Fast motions, slow motions, and implications for receptor binding

MATTHEW P. CRUMP,[1] LEO SPYRACOPOULOS,[2] PIERRE LAVIGNE,[1] KEY-SUN KIM,[3] IAN CLARK-LEWIS,[4] AND BRIAN D. SYKES[1,2]

[1]The Protein Engineering Network of Centres of Excellence (PENCE) and Department of Biochemistry, University of Alberta, Edmonton, Alberta T6G 2S2, Canada
[2]MRC Group in Protein Structure and Function, Department of Biochemistry, University of Alberta, Edmonton, Alberta T6G 2H7, Canada
[3]Structural Biology Center, Korean Institute of Science and Technology (KIST), P.O. Box 131, Cheongyang, Seoul 130-650, Korea
[4]Biomedical Research Centre and Department of Biochemistry and Molecular Biology, University of British Columbia, Vancouver, British Columbia V6T 1Z3, Canada

(RECEIVED June 8, 1999; ACCEPTED July 30, 1999)

Abstract

Eotaxin is a member of the chemokine family of about 40 proteins that induce cell migration. Eotaxin binds the CC chemokine receptor CCR3 that is highly expressed by eosinophils, and it is considered important in the pathology of chronic respiratory disorders such as asthma. The high resolution structure of eotaxin is known. The 74 amino acid protein has two disulfide bridges and shows a typical chemokine fold comprised of a core of three antiparallel β-strands and an overlying α-helix. In this paper, we report the backbone dynamics of eotaxin determined through ^{15}N-T_1, T_2, and $\{^1H\}$-^{15}N nuclear Overhauser effect heteronuclear multidimensional NMR experiments. This is the first extensive study of the dynamics of a chemokine derived from 600, 500, and 300 MHz NMR field strengths. From the T_1, T_2, and NOE relaxation data, parameters that describe the internal motions of eotaxin were derived using the Lipari–Szabo model free analysis. The most ordered regions of the protein correspond to the known secondary structure elements. However, surrounding the core, the regions known to be functionally important in chemokines show a range of motions on varying timescales. These include extensive subnanosecond to picosecond motions in the N-terminus, C-terminus, and the N-loop succeeding the disulfides. Analysis of rotational diffusion anisotropy of eotaxin and chemical exchange terms at multiple fields also allowed the confident identification of slow conformational exchange through the "30s" loop, disulfides, and adjacent residues. In addition, we show that these motions may be attenuated in the dimeric form of a synthetic eotaxin. The structure and dynamical basis for eotaxin receptor binding is discussed in light of the dynamics data.

Keywords: backbone ^{15}N dynamics; CC chemokine; conformational exchange; eotaxin; monomer–dimer equilibrium

Eotaxin (Griffiths-Johnson et al., 1993; Jose et al., 1994) is a member of the chemotactic cytokine (chemokine) family of proteins involved in the immune and inflammatory response. The chemokines promote recruitment of different subpopulations of leukocytes through their binding and activation of seven transmembrane (7TM) receptors (Baggiolini et al., 1997 and references therein). The CC chemokine eotaxin is specific for the CCR3 receptor that is distributed on eosinophils and basophils (Jose et al., 1994; Kitaura et al., 1996; Ponath et al., 1996) and T helper 2 (T_H2) cells (Sallusto et al., 1997). It is thought that the stimulation and sustainment of an allergic reaction requires T_H2 cells that provide a source of IL-4 and IL-5 for growth and stimulation of eosinophils and basophils (Corrigan & Kay, 1992). The specificity of eotaxin for CCR3 on these three cell types may allow it to play a coordinating role in the infiltration of these leukocytes into the airways and has therefore been recognized as central to the pathogenesis of chronic respiratory disorders such as asthma.

Members of both the CXC and CC chemokine families have been the subject of intensive structural and functional studies in an attempt to understand receptor binding determinants. Three-

Reprint requests to: Brian D. Sykes, The Protein Engineering Network of Centres of Excellence (PENCE) and Department of Biochemistry, University of Alberta, Edmonton, Alberta T6G 2S2, Canada; e-mail: brian.sykes@ualberta.ca.

Abbreviations: BPTI, bovine pancreatic trypsin inhibitor; CPMG, Carr-Purcell-Meiboom-Gill; CSA, chemical shift anisotropy; HPLC, high-performance liquid chromatography; HSQC, heteronuclear single quantum coherence; NMR, nuclear magnetic resonance; NOE, nuclear Overhauser effect; NOESY, NOE spectroscopy; RMSD, root-mean-square deviation; T_1, longitudinal relaxation time; T_2, transverse relaxation time; $D_\parallel/D_\perp$, rotational diffusional anisotropy defined as $2D_z/(D_x + D_y)$ where D is the rotational diffusion coefficient.

dimensional structural studies by NMR have revealed that monomeric chemokine structures are remarkably homogeneous and differences that may be attributable to receptor specificity are certainly not obvious (Fairbrother & Skelton, 1996). A standard chemokine fold appears to consist of three antiparallel β-strands (β1, β2, and β3) and an overlying α-helix. The remainder of the protein consists of an apparently disordered N-terminal region, an extended N-terminal loop, a "30s" loop connecting β1 and β2, the 40s turn connecting β2 and β3, and the 50s turn connecting β3 to the C-terminal α-helix. Numerous structure-function studies have shown the N-terminal region preceding the CC or CXC motif to be the most important region for receptor binding/activity (Clark-Lewis et al., 1994, 1995; Gong et al., 1996), yet this region appears unstructured in solution structures of monomeric subunits (Kim et al., 1996; Crump et al., 1997, 1998). The N-terminal loop (succeeding the CXC or CC motif and preceding the first β-strand) has been shown to be important for receptor specificity and contributions to binding (Clark-Lewis et al., 1994, 1995; Schraufstätter et al., 1995; Lowman et al., 1996; Pakianathan et al., 1997). In addition the disulfide bridges and the 30s loop may play a very highly tuned structural role (Clark-Lewis et al., 1994, 1995; Rajarathnam et al., 1999). In all, a central core or scaffold of β-strands and an α-helix appears to be surrounded by functionally important regions of the protein.

We report the first detailed backbone ^{15}N NMR relaxation measurements of eotaxin, the first such study on a human CC chemokine. We have previously reported the three-dimensional structure of synthetic eotaxin using multidimensional NMR methods that revealed a predominantly monomeric species at the concentration studied (K_d = 0.0085, 30 °C, pH 5.0, NaOAc) and a typical chemokine fold (Crump et al., 1998). However, this does not provide details on the rotational and internal dynamics of the protein and in particular, information of importance in functionally sensitive regions. Heteronuclear NMR experiments provide T_1, T_2, and {^{1}H}-^{15}N (steady state heteronuclear Overhauser enhancement) relaxation data at multiple protein sites (for reviews on ^{15}N NMR relaxation see Palmer, 1993; Wagner, 1993). Relaxation data are interpreted in the context of motional models, in this case the Lipari & Szabo model-free formalism (Lipari & Szabo, 1982a, 1982b). This allows the extraction of an overall correlation time (τ_m), internal correlation times (τ_e), and order parameters (S^2) for backbone N-H bond vectors. This study reveals that although the core of the protein is well defined on the subnanosecond to picosecond timescale, the more functionally sensitive regions identified in other chemokines show motions on various timescales. Three samples were used; a recombinant uniformly ^{15}N labeled sample with a GSHM N-terminal extension and two synthetic samples (N1 and N2) with site specific ^{15}N labels. We show that the recombinant sample is monomeric and the N- and C-termini undergo rapid subnanosecond timescale motions. The N-loop shows reduced order parameters and the 30s loop and adjacent residues in the N-terminus show conformational exchange. The synthetic samples are in a monomer/dimer equilibrium that allows the comparison of the backbone dynamics for several specifically labeled residues in the monomeric and dimeric form.

Results

^{15}N-T_1, T_2, and NOE analysis

The backbone amide ^{15}N and ^{1}H chemical shifts for eotaxin have been deposited in BioMagResBank with access code 4155. At 500 and 600 MHz, ^{15}N relaxation data for 61 out of 74 residues could be obtained. The missing 13 residues were 8 prolines (no amide proton), Cys34 and Lys67 (signal overlap), Gly1, Cys10, and Phe11 (no signal observed). Significantly fewer peaks were characterized at 300 MHz due to poor signal to noise giving 47 T_1 data points and 54 T_2 data points. Characteristic fits for the T_1 and T_2 data are shown in Figure 1. Figure 2A shows T_1 relaxation data at 300, 500, and 600 MHz and the associated errors in fitting the decay curves.

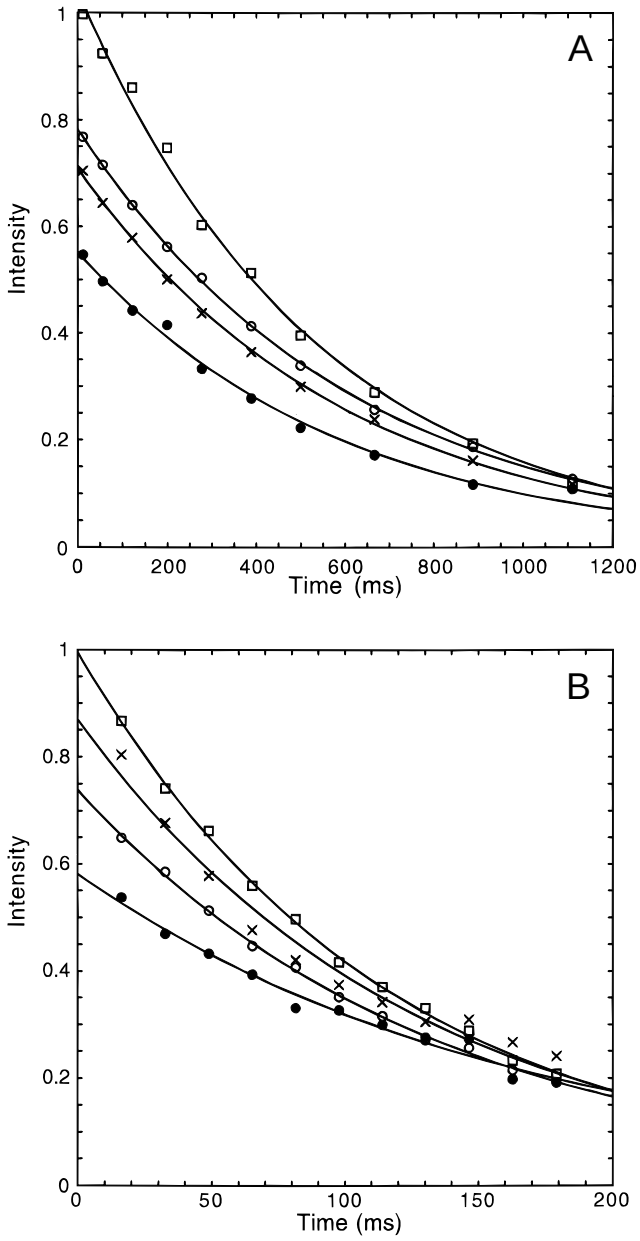

Fig. 1. Best and worst fits of ^{15}N relaxation data. Shown are fitted decay curves for (**A**) ^{15}N-T_1 and (**B**) ^{15}N-T_2 at 500 and 600 MHz. The following residues are shown that fitted with approximately 1% error in the final T_1 or T_2 and are among the best fits of the data: T_1^{600} (Lys47 609 (±4.4) ms{○}), T_1^{500} (Arg27 411 (±5) ms {□}), T_2^{600} (Thr43 133 (±1.7) ms {○}), T_2^{500} (Gln36 118 (±1.8) ms {□}). Also shown are representative plots of the some of the worst fit data: T_1^{600} (Leu18 584 (±21) ms {●}), T_1^{500} (Leu13 463 (±18) ms {×}), T_2^{600} (Leu18 167 (±8) ms {●}), T_2^{500} (Ile29 131(±8) ms {×}).

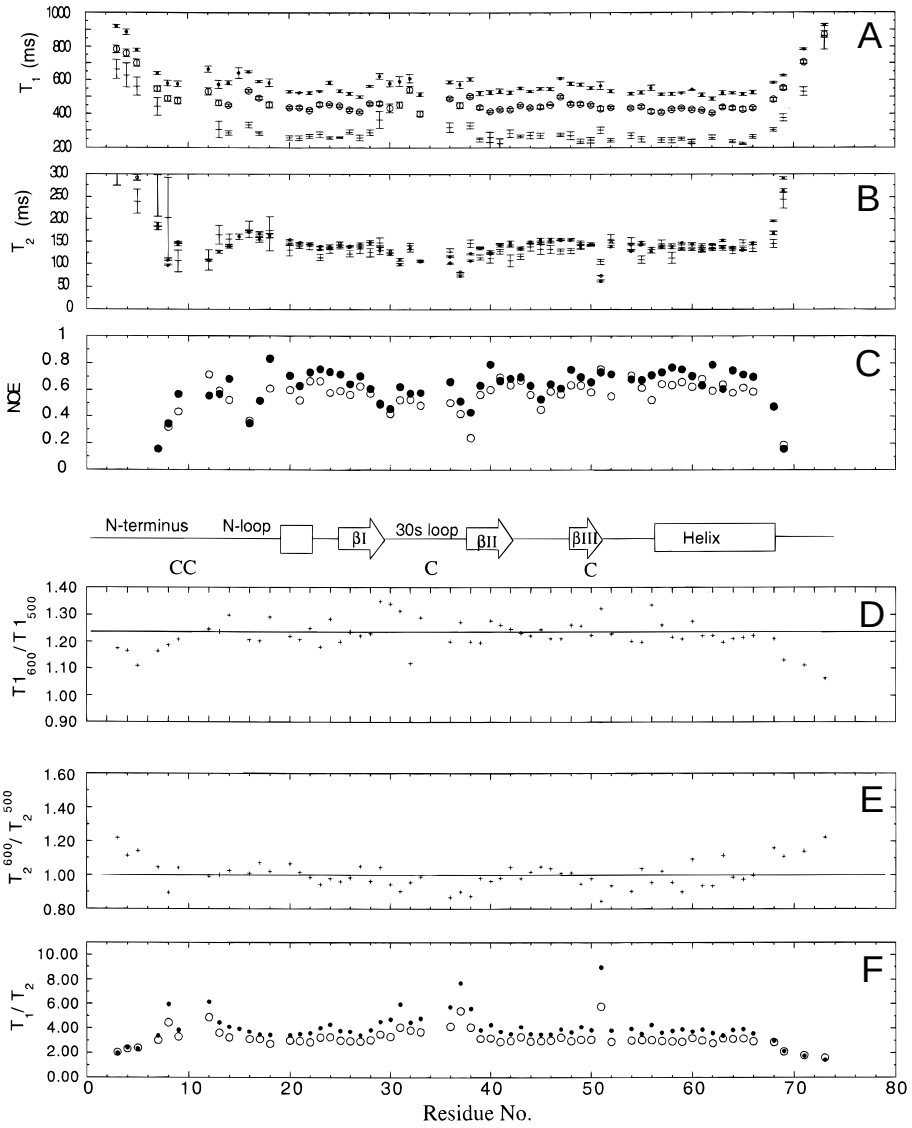

Fig. 2. Relaxation data for eotaxin at three magnetic fields. Plots of (**A**) ^{15}N-T_1, (**B**) ^{15}N-T_2 at 300 {+}, 500 {○}, 600 {●} MHz and (**C**) NOE at 500 and 600 MHz (no 300 MHz NOE data are reported due to the poor signal to noise ratio that was obtained in the proton saturation half of the experiment). Elements of secondary structure are shown as determined from the coordinates of the average minimized NMR structure determined by Crump et al. (1998). An arrow defines a β-strand, a box a helix, and a black line indicates coil or loop structure (Secondary structure: 3_{10} helix (19–22), β1 (25–29), β2 (38–43), β3 (48–51), and helix-1 (57–68)). Also shown are plots of (**D**) T_1^{600}/T_1^{500}, (**E**) T_2^{600}/T_2^{500}, and (**F**) T_1/T_2 for 600 (●) and 500 (○) MHz. Lines are shown on **D** and **E** for the theoretical ratios $T_1^{600}/T_1^{500} = 1.25$ and $T_2^{600}/T_2^{500} = 0.97$. The plots reveal the superior quality of the 500 and 600 MHz data, which were used for a complete isotropic and anisotropic relaxation analysis.

The average T_1^{600} for all residues was 583 ± 93 ms with an average error of 11 ms, the average T_1^{500} was 478 ± 95 ms with an average error of 10 ms, and the average T_1^{300} was 316 ± 128 ms with an average error of 21 ms. Residues for which internal motion affects the T_1 values were identified by a NOE less than 0.65 or 0.60 at 600 and 500 MHz, respectively. These included residues 3–13, 15–17, 28–33, 37, 38, 45, 47, 63, and 68–73 at 600 MHz, 3–9, 16–17, 21, 29, 31–38, 44–47, 49, 68–73 at 500 MHz. Excluding these residues the average T_1^{600} was 541 ± 28 ms with an average error of 9.7 ms and the average T_1^{500} was 434 ± 15 ms with an average error of 8 ms. NOE data could not be collected at 300 MHz, principally due to poor signal to noise ratios in the proton saturated (with NOE) {^{1}H}-^{15}N HSQC. Selecting residues from the 300 MHz data that had already been identified as rigid gave $T_1^{300} = 258.7 \pm 17.2$. The average T_1^{600}/T_1^{500}, T_1^{600}/T_1^{300} and T_1^{500}/T_1^{300} was 1.24 ± 0.035, 2.08 ± 0.15, and 1.69 ± 0.12 (Fig. 2D).

Figure 2B shows T_2 data recorded at multiple fields. The average T_2^{600} was 164 ± 97 ms over all residues and 138 ± 16 ms (average error 2.5 ms) over the residues with NOE > 0.65 (140 ± 9 ms with the exception of Ala51, which displayed an unusually small T_2). The average T_2^{500} was 161 ± 76 ms over all residues and 139 ± 15 ms (average error of 2.3 ms) over residues with NOE > 0.60 (140 ± 9.5 ms excluding Ala51) and the average T_2^{300} was

173 ± 102 ms over all residues and $T_2^{300} = 135 \pm 17$ (average error of 10 ms) over those residues selected with NOE > 0.60 at 500 MHz (136 ± 16 ms without Ala51). The average T_2^{600}/T_2^{500} (Fig. 2E), T_2^{600}/T_2^{300}, and T_2^{500}/T_2^{300} was 0.98 ± 0.05 ms, 1.05 ± 0.13 ms, and 1.05 ± 0.12 ms, respectively.

The average NOE^{600} is 0.52 ± 0.34 over all residues and 0.62 ± 0.14 over all residues with a positive NOE. The average NOE^{500} is 0.48 ± 0.40 over all residues and 0.58 ± 0.15 for residues with a positive NOE.

The average T_1^{600}/T_2^{600}, T_1^{500}/T_2^{500}, and T_1^{300}/T_2^{300} was 3.83 ± 0.27, 3.09 ± 0.15, and 1.97 ± 0.30, respectively (Fig. 2F).

Determination of the overall correlation time of eotaxin

The backbone ^{15}N relaxation data were interpreted with the Lipari–Szabo method that interprets relaxation data in a model independent formalism. The information content of the relaxation data is expressed in terms of a generalized order parameter S^2 that describes the degree of spatial restriction of a bond vector and τ_e, an effective correlation time for the fast rate ($\tau_e < 0.3$ ns) of internal bond vector motion. If a τ_m can be defined, S^2 and τ_e may be adjusted to account for internal motions. The overall correlation time was determined for recombinant eotaxin using 500 and 600 MHz data sets independently. Initially an optimal τ_m was calculated on a per residue basis by minimizing the difference between the experimental and the calculated T_1, T_2, and NOE (Equation 9) using the isotropic spectral density function given by Equation 8 (Farrow et al., 1994). Once optimum τ_m values were calculated for each residue, an optimum average τ_m was calculated. The τ_m was calculated to be 5.50 ms and 5.56 ms at 600 and 500 MHz, respectively.

Model-independent analysis of backbone dynamics

From the measured T_1, T_2, and NOE relaxation data, parameters that describe the internal motions of eotaxin were determined using the model-free analysis under the assumption of isotropic tumbling (Lipari & Szabo, 1982a, 1982b). Appropriate models of spectral density functions were selected for each residue. These included $S^2 - \tau_m$, $S^2 - \tau_m - \tau_e$, $S^2 - \tau_m - R_{ex}$, and $S^2 - \tau_m - \tau_e - R_{ex}$ models and a two-timescale model (Clore et al., 1990a, 1990b) as defined in Materials and methods. Models were fitted separately with 500 and 600 MHz data allowing the final model free parameters to be independently determined by two datasets. Figures 3A and 3B show results for all residues fitted with the $S^2 - \tau_m - \tau_e$ model at both 500 and 600 MHz. τ_m was fixed at 5.50 and 5.56 ns for the 600 and 500 MHz data, respectively. The average S^2 at 600 MHz for residues with $NOE^{600} > 0.65$ is 0.83 (±0.04) and at 500 MHz with $NOE^{500} > 0.60$ is 0.82 (±0.03). The results agree well between the 500 and 600 MHz data.[5] Not surprisingly, the N- and C-termini show pronounced reductions in S^2, indicating fast motions in the subnanosecond timescale. Lower S^2 values are also seen throughout the N-loop with the exception of Leu13. In addition, there are also reduced S^2 values throughout the 30s loop connecting β1 and β2. The core of eotaxin (β1, β2, β3, and the α-helix) is well defined, containing the majority of residues with NOE^{600} or NOE^{500} greater than 0.65 and 0.60, respectively, and S^2 values around or greater than 0.80. At 600 MHz, 36 residues were fit well with either the $S^2 - \tau_m$ or $S^2 - \tau_m - \tau_e$ models (T7, C9, A14, N15, R16, K17, I18, Q21, R22, L23, S25, Y26, R28, G32, V39, F41-C50, D52, K54, W57-M62, Y64, L65, D66). Four residues could not be fit by any model (A3, S4, T71, K73). At 500 MHz, 39 residues were fit with either the $S^2 - \tau_m$ or $S^2 - \tau_m - \tau_e$ models (S4, L5, K17, I18, L20, Q21, R22, L23, S25, Y26, R27, R28, T30, V39, I40–K42, K44–C50, D52, K54, K55, W57-D66, S68), and 3 residues could not be fit by any model (terminal residues A3, T71, K73).

For those residues that did not fit well to the $S^2 - \tau_m$ or $S^2 - \tau_m - \tau_e$ models, alternative models were assumed (i.e., $S^2 - \tau_m - \tau_e - R_{ex}$ and the two-timescale model). In total, 14 and 17 residues required additional models at 600 and 500 MHz, respectively. A suitable model was selected according to the criteria of Farrow et al. (1994) and Gagné et al. (1998). These include (1) that relaxation parameters must be fit within 95% confidence levels, (2) that new parameters in the fit are significant (a value larger than its associated error), and (3) the model must agree at multiple fields. For the $S^2 - \tau_m - \tau_e - R_{ex}$ model, 10 residues satisfied these criteria (Fig. 3C) (Thr8, Asn12, Glu24, Ile29, Ser31, Lys33, Gln36, Lys37, Ala38, and Ala51). Residues Ile29 to Ala38 form an almost contiguous stretch of residues requiring an R_{ex} term (Gly32 and Thr30 required R_{ex} terms at only one field strength and Cys34 and Pro35 could not be measured). Thr8 and Asn12 are on either side of the disulfide bridges that connect the N-terminal region to the 30s loop and β3 (see schematic in Fig. 3). Ala51 is adjacent to Cys50 connecting β3 to the N-terminus and is in close proximity to Ala38 and Val39 on β2. Thus these residues appear to form a grouping around the 30s loop and disulfide bridges that experience conformational exchange.

The presence of conformational exchange can be validated by the ratio of R_{ex} terms at different field strengths. Theoretically the $R_{ex}^{600}/R_{ex}^{500}$ ratio should be equal to $600^2/500^2$ or 1.44. The ratio for the 30s loop is 1.36 ± 0.18 and in every case the R_{ex}^{600} is greater than R_{ex}^{500}. As shown in Figure 3C, the values of R_{ex}^{600} and R_{ex}^{500} throughout the 30s loop are large, ranging from 1.4 to 6.8 s^{-1} and 1.11 to 5.65 s^{-1}, respectively and are significant with respect to their associated error (0.34 ± 0.10 at 600 MHz and 0.38 ± 0.13). Ala51 shows the largest R_{ex} terms of 8.96 and 6.21 s^{-1} at 600 and 500 MHz, in a ratio of exactly 1.44. Thr8 and Asn12 have $R_{ex}^{600}/R_{ex}^{500}$ ratios greater than one although at 1.21 and 1.06, respectively, they are slightly lower than expected. These results, however, strongly suggest the presence of slow (micro to millisecond) conformational exchange within the 30s loop and Ala51 that may also be related to a slow exchange involving residues Thr8 and Asn12.

The final isotropic spectral density function required was the two-timescale model reported by Clore et al. (1990a, 1990b) and described by Equation 11. Using the above criteria, only one residue adequately fit this model, Ser69. According to the family of 32 NMR structures, Ser69 is situated at the C-terminal part of the α-helix and shows angular order parameters of $\boldsymbol{S}(\phi) = 0.97$ and $\boldsymbol{S}(\psi) = 0.75$ ($\boldsymbol{S}, \boldsymbol{S} = 1$ if the angle is identical in every structure and $\boldsymbol{S} = 0$ if the angle is completely undefined; Hyberts et al., 1992). The NMR structures also suggest that subsequent residues show further reductions in $\boldsymbol{S}(\phi)$ and $\boldsymbol{S}(\psi)$ and that the helix begins to fray at Ser69 (Crump et al., 1998). It is not surprising therefore that

[5] Values for τ_e are extremely sensitive to the measured NOE (Kay et al., 1989) and systematically high NOE^{600} values lead to an observed reduction of τ_e values at 600 MHz compared to 500 MHz. For a fixed τ_m of 5.50 ns and S^2 of 0.85, the calculated NOE^{600}/NOE^{500} varies from 1.04 to 1.01 as τ_e changes from 0 to 100 ps (Gagné et al., 1998). This compares to the actual ratio of 1.14 ± 0.12 over residues in the core of eotaxin.

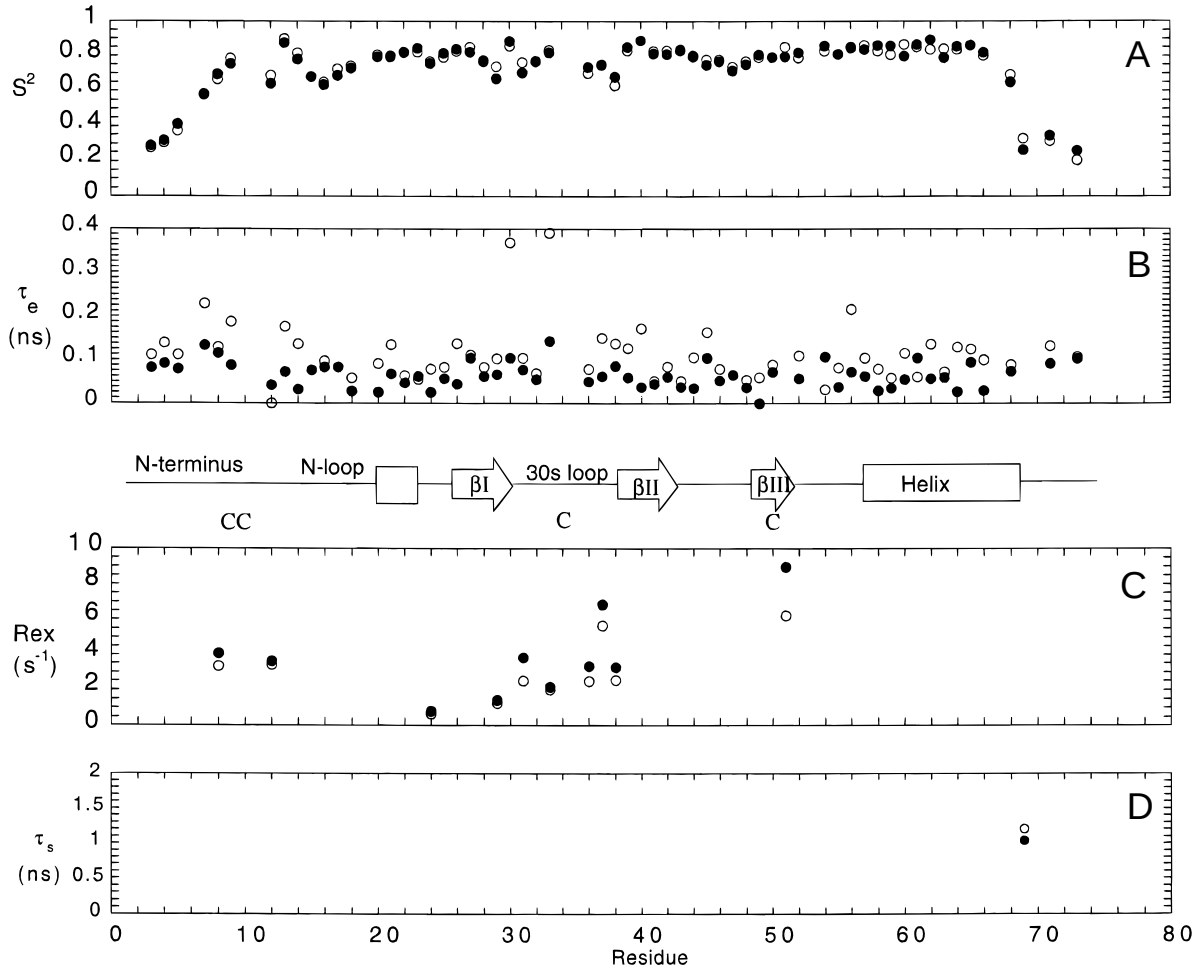

Fig. 3. Graphical representation of dynamics parameters derived from the Lipari and Szabo model free analysis (Lipari & Szabo, 1982a, 1982b). **A:** Order parameters (S^2). **B:** Internal correlation times (τ_e). **C:** Conformational exchange terms (R_{ex}). **D:** Two-timescale (τ_s) parameters are plotted as a series of sequential plots. (●) indicates data at 600 MHz and (○) indicates data at 500 MHz. A fit to the $S^2 - \tau_m - R_{ex}$ or the two-timescale model was only deemed significant by several criteria described in the text so R_{ex} and τ_s are shown only for those residues. Error bars for S^2 are smaller than the symbols used for plotting and are not shown.

Ser69 shows a two-timescale motion with fast motions and an additional slow internal motion characterized by a τ_s of ~1.0 ns.

Rotational diffusion anisotropy

It has been reported that fitted R_{ex} terms can arise from rotational diffusion anisotropy but be mistakenly interpreted as conformational exchange (Tjandra et al., 1995). This can occur, for example, in helices whose NH vectors lie along a similar axis to the unique rotational diffusion axis of a protein with a prolate shape, leading to elevated ^{15}N-T_1/T_2 ratios that can be mistaken as a increase in $1/T_2$ by R_{ex} (Equation 10). To ensure that the data had been interpreted correctly, a model for rotational diffusional anisotropy was considered for eotaxin. Although the principal moment of the inertia tensor for eotaxin is 1.00:0.80:0.73 (1.00:0.88:0.69 for residues 8–74) suggests that the protein tumbling should be approximately isotropic, the recent report of large rotational diffusion anisotropy in vMIP-II ($D_\parallel/D_\perp = 1.5$, prolate) (LiWang et al., 1999) warranted a similar study for eotaxin.

Rotational diffusion anisotropy was analyzed for eotaxin in a similar fashion to Tjandra et al. (1995). The 500 and 600 MHz data sets were used for the analysis and residues were selected on the basis outlined by Tjandra et al. (1995, 1996). Briefly, residues were rejected if (1) the NOE^{600} or NOE^{500} smaller than 0.65 or 0.60, respectively; (2) they were located in loops or turns; or (3) the residues were potentially undergoing conformational exchange identified with the following condition:

$$(\langle T_2\rangle - T_{2,n})/\langle T_2\rangle - (\langle T_1\rangle - T_{1,n})/\langle T_1\rangle > 1.5\sigma \qquad (1)$$

where $T_{2,n}$ is the T_2 of residue n, T_2 is the average T_2, and σ is the standard deviation of the average $(\langle T_2\rangle - T_{2,n})/\langle T_2\rangle - (\langle T_1\rangle - T_{1,n})/\langle T_1\rangle$. Using these conditions a set of 32 residues was selected from the 500 and 600 MHz data sets and analyzed separately. The data were fitted to three models for the diffusion tensor: isotropic, axially symmetric, and fully anisotropic. The coordinates of the average minimized NMR structure of eotaxin were used for the analysis (Brookhaven accession code 1EOT). The results of the isotropic fit and the axially symmetric fits are shown in Table 1. In stark contrast with vMIP-II, the axially symmetric model predicts $D_\parallel/D_\perp$ of 0.87 and 0.94 (oblate) at 600 and 500 MHz, respectively.

Table 1. *Rotational diffusion anisotropy of eotaxin*

	600 MHz		500 MHz	
	Isotropic	Axially Symmetric	Isotropic	Axially Symmetric
θ[a]	—	22	—	24
ϕ[a]	—	−100.8	—	−134.8
$D_{\|}/D_{\perp}$[b]	1	0.87	1	0.94
χ^2[c]	148	117	78.11	73.8
χ_v^2[d]	4.78	4.18	2.52	2.64
F_x[e]	—	2.50	—	0.52

[a]Angles describing the orientation of the diffusion tensor in the identical coordinate frame as the deposited minimized average coordinates for eotaxin (Brookhaven Protein Data Bank access code 1EOT).
[b]Defined as $2D_z/(D_x + D_y)$.
[c]Error function, $\chi^2 = \sum_n (T_{1,e}/T_{2,e} - T_{1,c}/T_{2,c})^2/\sigma^2_{T_1/T_2}$.
[d]Reduced error function, $\chi_v^2 = \chi^2/(N - m)$.
[e]Test for adding x variables to the fitting procedure (Bevington & Robinson, 1992).

A statistical F-test (Bevington & Robinson, 1992) was used to assess whether the fits occurred by chance with the inclusion of additional parameters. At 600 MHz the probability that the improvement in the fit for the axially symmetric model is 8.0×10^{-2} that in this case justifies the application of this model. However, for the 500 MHz data the probability that the improvement occurred by chance is 0.67 and certainly does not represent a significant improvement over the isotropic model. Considering just the 600 MHz data set, there was no significant improvement in fits when the D_x/D_y ratio was allowed to vary with a fully anisotropic model. Figure 4 shows eotaxin as a ribbon diagram with the principal diffusion axis perpendicular to the page. In conclusion, the anisotropy is small and does not account for the exchange terms and reduced T_2 values we observed. Therefore, for the remainder of the manuscript interpretation of the results will be in the context of isotropic models.

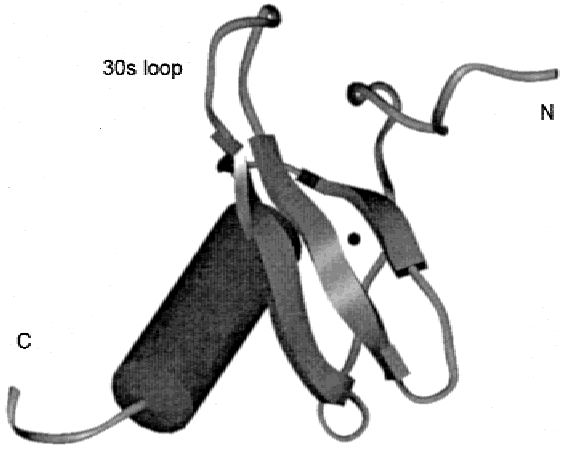

Fig. 4. Ribbon structure of the minimized average structure of eotaxin relative to the axially symmetric diffusion tensor determined at 600 MHz. Note that in this orientation $D_{\|}$ is perpendicular to the plane of the page.

Comparison of monomer and dimer dynamics

As discussed in a previous paper (Crump et al., 1998), synthetic eotaxin exhibits a monomer/dimer equilibrium that is not observed in the recombinant sample presumably due to the GSHM extension that interferes with the dimerization interface. To investigate the dynamics of eotaxin in the monomeric state vs. the dimeric state, we utilized synthetic samples of eotaxin (termed N1 and N2, see Materials and methods).

In analyzing relaxation data for the two peptides, two situations arose. First, the monomer and dimer backbone nitrogen and amide proton resonances could be degenerate leading to a single correlation peak on the HSQC spectrum. For five residues (Leu20, Val23, Val39, Val58, and Ser61), the ^{1}H-^{15}N correlation of the monomer coincides with the equivalent dimer correlation. Secondly, separate resonances were observable in some cases for the monomer and dimer species. Interestingly, this occurred for three residues, Ser31, Gly32, and Ala51, implying a possible structural/dynamical change for these residues upon dimerization. Figure 5A shows an expansion from a ^{1}H-^{1}H NOESY of a 3 mM sample of unlabeled eotaxin that was used to characterize the monomer/dimer equilibrium (Crump et al., 1998). The NOEs connecting the Ala51 amide to the Cys50 Cα proton are labeled for the both the monomeric and dimeric state. Exchange peaks are labeled with an asterisk. The amide shifts of Ala51 in the monomer and dimer (9.70 and 9.82 ppm, respectively) are seen to correspond exactly with the two correlation peaks observed in the HSQC spectrum of N2 (Fig. 5B), which were subsequently assigned to monomer and dimer species. A similar analysis led to the identification of monomer and dimer resonances for Ser31 and Gly32.

For the second case, where resolvable monomer and dimer peaks are observed, it is evident that monomer–dimer exchange is in the slow exchange limit with respect to the chemical shift difference ($\Delta\delta$) (rad s^{-1}); $(\tau_{ex} \cdot \Delta\delta)^2 > 1$; $\tau_{ex} = \tau_M \cdot \tau_D/(\tau_M + \tau_D)$; where τ_M and τ_D are the lifetimes of the monomer and dimer, respectively. To characterize the monomer–dimer exchange, we assumed a simple model shown in Figure 6. The monomer and dimer are assumed to exchange at a given rate ($k_{ex} = k_{MD} + k_{DM}$) without passing through stable intermediate states. In addition, we recognize that there is additional exchange among internal states of the monomer and perhaps the dimer, but these are neglected initially.

According to Equation 2 (below), k_{ex} may be calculated by analysis of NOESY spectra (Fig. 5A) at given mixing times (t):

$$I_c/(I_d + (I_N/3)) = \{1 - \exp(-2k_{ex}t)\}/\{1 + \exp(-2k_{ex}t)\} \quad (2)$$

where I_c and I_d are the intensities of the exchange and diagonal peaks, respectively (Jeener et al., 1979). I_N is the intensity of the NOE cross peaks and the term $I_N/3$ is introduced to correct for the NOE depletion of the diagonal cross peak (Katoh et al., 1999). Analysis of NOESY spectra at 75 and 150 ms for Ala51 (that was well resolved) gave a k_{ex} of 1.0 s^{-1}.

The relaxation data were therefore interpreted in the limit where $\tau_{ex}/T_{1M,D}, \tau_{ex}/T_{2M,D} \gg 1$. In the first case, for overlapped monomer and dimer peaks, longitudinal and transverse relaxation rates are given by the bi-exponential decay of the signal intensity $I(t)$ in Equation 3,

$$I(t) = I(0)(p_D \exp(-t/T_{1,2D}) + p_M \exp(-t/T_{1,2M})) \quad (3)$$

where $I(0)$ is the initial signal intensity, $T_{1,2}$ is the longitudinal or transverse relaxation time for the dimer ($T_{1,2D}$) or monomer ($T_{1,2M}$),

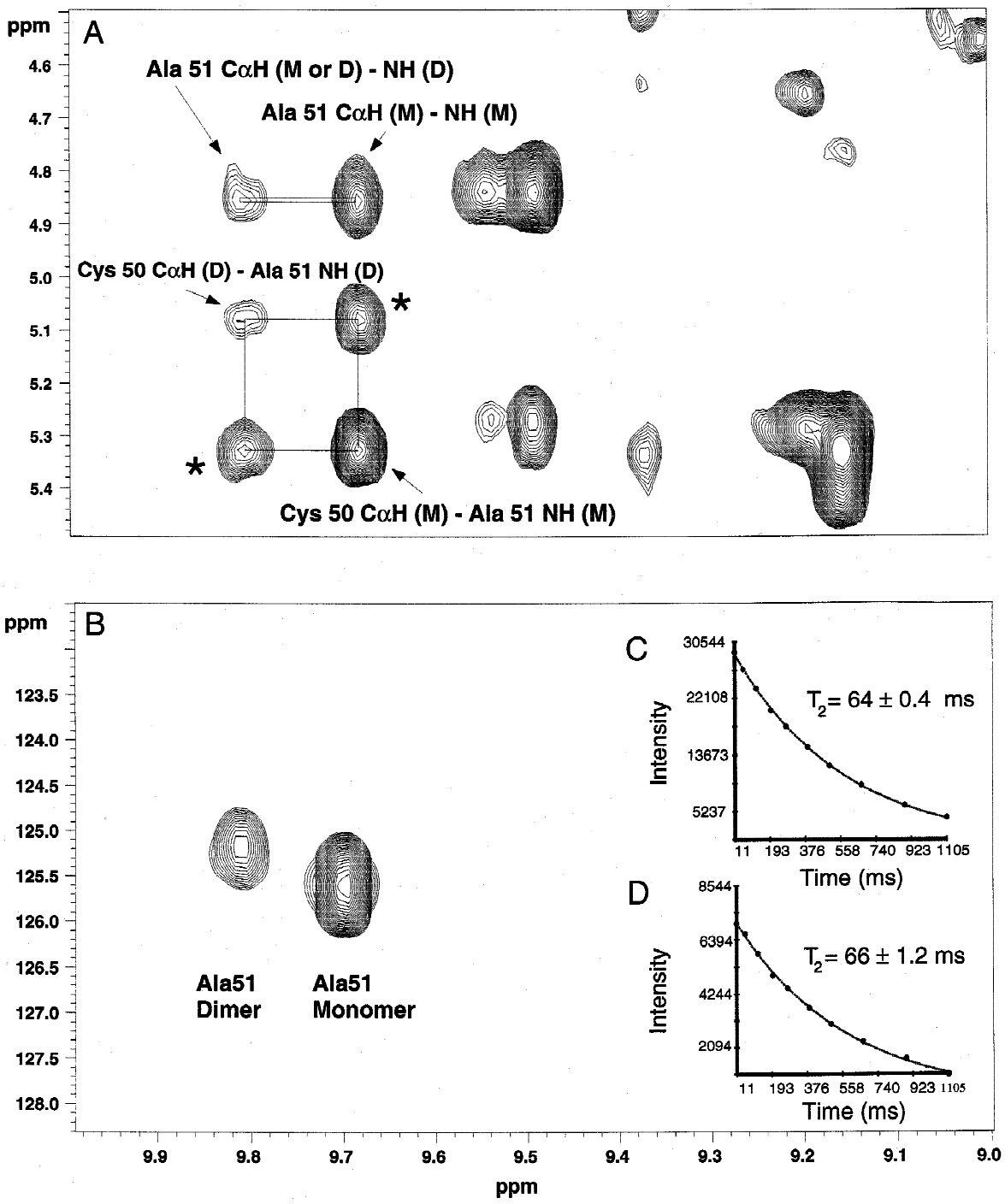

Fig. 5. Spectra demonstrating the exchange of eotaxin between monomeric and dimeric states. **A:** Expansion of a ^{1}H-^{1}H 2D-NOESY plot recorded on a 3 mM sample of unlabeled synthetic eotaxin at pH 5.0, 30 °C. The spectrum is annotated for Ala51 identifying the intraresidue and sequential NOE correlation peaks to the amide proton in the monomer (*M*) and dimer (*D*) species. Exchange peaks are marked with an asterisk. **B:** Expansion of the corresponding ^{1}H-^{15}N HSQC spectra of a specifically labeled eotaxin sample (N2) showing a correlation for Ala51 in both the monomeric and dimeric species. Exchange peaks are just resolved when plotted at low contour levels. Inserts **C** and **D** compare the decay curves for the Ala51 monomer and dimer resonances from a set of T_2 experiments with the N2 peptide.

and p_D, p_M are the populations of the dimer and monomer, respectively. Therefore, relaxation times for the dimer were extracted by fitting Equation 3 using p_D and p_M (determined from peak volumes in the HSQC, $p_M = 0.77$, $p_D = 0.23$) and the known transverse relaxation times determined from the recombinant sample for the monomer.

In the second case where clear monomer and dimer peaks were observable, the time evolution of the longitudinal magnetization is

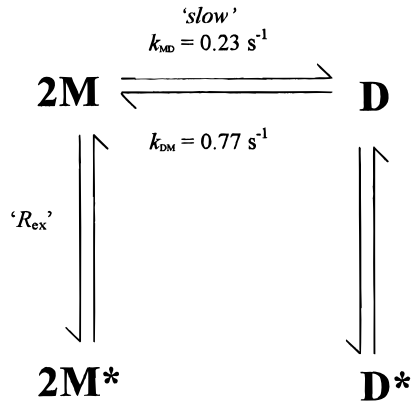

Fig. 6. A model for the exchange of eotaxin between monomer and dimer. *M* denotes eotaxin in the monomeric state and *D* denotes eotaxin in the dimeric state. A simple two-state exchange is depicted with forward rate (k_{MD}) and backward (k_{DM}) rate constants. In addition, the monomer is assumed to be in exchange with other internal states (M^*) that we have characterized as conformational changes on a microsecond to millisecond timescale, and these are assumed to be fast with respect to the exchange between monomer and dimer states. The possibility that these motions persist in the dimer is indicated by exchange with some state D^*.

formally given by the solutions of the Bloch equations modified for exchange between two states (McConnell, 1958; Farrow et al., 1995),

$$I_M(T) = I_M(0)\{-(\lambda_2 - a_{11})\exp(-\lambda_1 t) + (\lambda_1 - a_{11})\exp(-\lambda_2 t)\}/(\lambda_1 - \lambda_2) \quad (4)$$

$$I_M(D) = I_D(0)\{-(\lambda_2 - a_{22})\exp(-\lambda_1 t) + (\lambda_1 - a_{22})\exp(-\lambda_2 t)\}/(\lambda_1 - \lambda_2) \quad (5)$$

where $I_{M,D}$ is the intensity of the monomer or dimer peak, $\lambda_{1,2} = (\frac{1}{2})\{(a_{11} + a_{22}) \pm [(a_{11} - a_{22})^2 + 4k_{MD}k_{DM}]^{1/2}\}$, $a_{11} = 1/T_{1M} + k_{MD}$, and $a_{22} = 1/T_{1D} + k_{DM}$. k_{MD} and k_{DM} were calculated from k_{ex}, p_M, and p_D giving $k_{MD} = 0.23$ and $k_{DM} = 0.77$ s^{-1}. In the exchange limit where k_{MD} and k_{DM} are small and T_{1M} and T_{1D} are the same order of magnitude, to a first approximation, the Equations 4 and 5 simplify to Equations 6 and 7 for the monomer and dimer, respectively,

$$I_M(t) = I_M(0)\exp(-t/T_{1M}) \quad (6)$$

$$I_D(t) = I_D(0)\exp(-t/T_{1D}). \quad (7)$$

Similarly if the exchange is sufficiently slow that exchange line broadening is negligible, with the additional provisos that $\Delta\delta <$ 300 Hz and the spacing between successive ^{15}N 180° pulses in the CPMG sequence is equal to 900 μs, then meaningful transverse relaxation rates can be extracted from Equations 6 and 7 (Farrow et al., 1995).

The T_1 and T_2 values for specific residues in the monomer and dimer are summarized in Table 2. It can be seen that for the five core residues (Leu20, Val23, Val39, Val58, and Ser61) analyzed, the values obtained for T_1 in the dimer are larger than the monomer while the T_2 values are reduced, as expected for a larger molecular weight species. The ^{15}N backbone dynamics of the CC chemokine dimer MIP-1β have been reported (Laurence et al., 1998), and the values determined here for eotaxin are scattered around the average T_1 and T_2 values reported for the core residues of MIP-1β (MIP-1β averages, T_1 708 ± 51, T_2 85 ± 5). Returning to Figure 6, we are reminded that for several residues we have to consider additional exchange terms characterized by internal motions. These considerations are pertinent to the relaxation analysis of both Ser31 and Ala51, both of which showed reduced T_2 values that were

Table 2. *T_1 and T_2 relaxation times for monomeric and dimeric eotaxin*

	Derived relaxation parameters[a]					
Residue	T_1^{obs} [b]	T_1^M	T_1^D	T_2^{obs}	T_2^M	T_2^D
Leu20	587 ± 3	532 ± 8	*834 ± 80* [b]	123 ± 0.4	154 ± 2	*54 ± 10*
Leu23	582 ± 4	535 ± 4	*784 ± 52*	108 ± 1.0	132 ± 2	*40 ± 11*
Val39	560 ± 5	523 ± 12	*723 ± 79*	124 ± 0.6	135 ± 3	*90 ± 10*
Val58	547 ± 3	518 ± 9	*665 ± 52*	122 ± 0.8	133 ± 2	*89 ± 9*
Ser61	548 ± 4	511 ± 9	*707 ± 64*	118 ± 0.6	130 ± 2	*85 ± 9*
Residue	$T_{1,M}^{obs}$ [c]	T_1^M	$T_{1,D}^{obs}$	$T_{2,M}^{obs}$	T_2^M	$T_{2,D}^{obs}$
Ser31	—[d]	593 ± 38	—	100 ± 0.8	100 ± 4	*96 ± 2*
Gly32	—	609 ± 25	—	105 ± 0.8	134 ± 7	*103 ± 4*
Ala51	*569 ± 5*	568 ± 21	*583 ± 8*	64 ± 0.4	63 ± 2	*66 ± 1.2*

[a]The top portion of the table describes experimental T_1 and T_2 values and derived parameters for those residues that showed overlapped monomer and dimer resonances. The bottom portion of the table describes T_1 and T_2 values and derived parameters for those residues where distinct resonances were observed for the monomer and dimer species. All values derived for the dimer are italicized.

[b]T_n^{obs} represents the observed T_1 or T_2 of an overlapped monomer-dimer peak fitted to a mono-exponential decay. T_1^M and T_2^M are the actual experimental values determined from the recombinant, monomeric sample, while T_1^D and T_2^D values shown in italics are values for the dimer obtained from fitting the decay to a bi-exponential with the known T_1^M and T_2^M values. Errors in T_1^D and T_2^D were estimated by including the error in T_1^M and T_2^M and a 5% uncertainty in the K_d for the monomer–dimer equilibrium.

[c]$T_{1,M}^{obs}$ and $T_{2,M}^{obs}$ are the observed T_1 and T_2 values for the monomer resonance, and $T_{1,D}^{obs}$ and $T_{2,D}^{obs}$ are the observed T_1 and T_2 values for the dimer resonance determined from fitting to a mono-exponential as described in results. T_1^M and T_2^M are again the actual values measured for the monomeric recombinant sample.

[d]No T_1 measurements were made for the N1 peptide.

attributable to conformational exchange. The transverse relaxation times for Ser31 and Ala51 are 100 and 63 ms, respectively, in the monomer and 96 and 66 ms in the dimer. Interestingly, we note that there is much less line broadening of the dimer peaks with respect to the monomer despite the increased molecular weight. In fact, they both show transverse relaxation rates typical of a "core" residue in the dimer. To clarify these results, potential T_2 values were simulated for an eotaxin dimer. This requires a value for the rotational correlation time (τ_m) of the dimer. Although we cannot extract an exact τ_m for the eotaxin dimer due to limited information, the τ_m approximately doubled from monomer to dimer in a study of MIP-1β (Laurence et al., 1998; 4.6 vs. 8.6 ns). For eotaxin, Val39, Val58, and Ser61 that are considered reliable "core" residues show an average T_1/T_2 of 7.9 ± 0.32 in the dimer, double the average in the monomer (3.83 ± 0.27). To a first approximation, it can be assumed that τ_m is doubled in the eotaxin dimer. Figure 7 shows simulated T_2 values ($S^2 = 0.85$, $\tau_e = 0$) for a τ_m of between 8 and 12 ns and R_{ex} values that are typically observed in the monomer (between 0 to 8 s^{-1}). We see that a τ_m of ~10 ns and $R_{ex} = 0$ gives T_2 values of ~85 ms, close to the "core" values for Val39, Val58, and Ser61. If the same slow motions were present in the dimer as the monomer, we would expect a diminished T_2 for Ala51 (where we identified an exchange term of ~8 s^{-1}) of approximately 50 ms. Similarly for Ser31 (R_{ex} in the monomer ~4 s^{-1}), a T_2 of ~65 ms is expected. The T_2 value of 66 ms for Ala51 ($S^2 = 0.85$) in the dimer can only be derived if the R_{ex} term is significantly reduced (from 8 to 4 s^{-1}) (Fig. 7). Similarly for Ser31, the T_2 value of 96 ms may be achieved by assuming an S^2 of 0.75 (as in the monomer) and reducing the R_{ex} term to close to 0. To verify these results, one dataset for the N2 peptide was recorded as 500 MHz so the field dependence of the R_{ex} terms in the dimer could be checked. For Ala51 the T_2 for the dimer was 78 ms, corresponding to a reduction of R_{ex} to about 2 s^{-1}. The ratio $R_{ex}^{600}/R_{ex}^{500}$ is therefore ~2 and agrees with the theoretical scaling of 1.44 with magnetic field strength. Both results are consistent with attenuation of slow motions upon dimerization.

Discussion

Eotaxin is a human CC chemokine that is apparently specific for CCR3 as it does not bind any of the other known functional mammalian chemokine receptors. Eotaxin is a potent chemoattractant for eosinophils, and it has been proposed that it could be important for allergic responses, particularly in the lung (Griffiths-Johnson et al., 1993; Jose et al., 1994; Kitaura et al., 1996; Ponath et al., 1996) where eosinophils predominate. Other molecules can also bind CCR3 but eotaxin is particularly special in its potency. In addition, eotaxin activates basophils and lymphocytes of the TH2 category that are involved in allergic reactions (Sallusto et al., 1997). Blockade at this level has potential in the treatment of chronic respiratory disorders such as asthma, and hence there is considerable interest in the structure/function relationships of eotaxin and its selectivity for CCR3. We have performed extensive relaxation measurements for eotaxin to understand its internal dynamics and their relationship to structure/function. These are discussed in detail below with relation to the structure and function of the chemokine family.

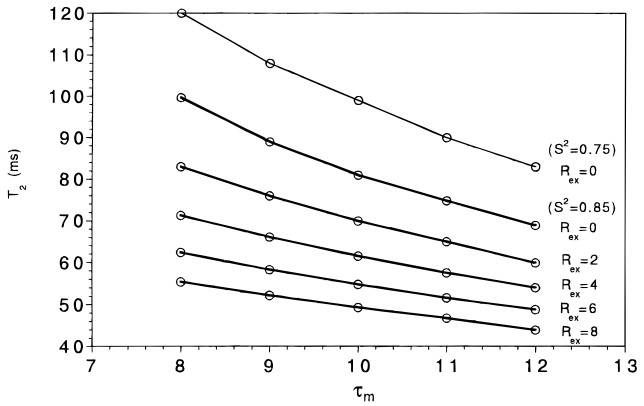

Fig. 7. Plots simulating the expected T_2 relaxation times for a given τ_m and R_{ex}. An isotropic tumbling model was assumed, and the parameters S^2 and τ_e were fixed at 0.85 and 0 ps, respectively.

Rotational correlation time

The rotational correlation time of eotaxin was determined to be 5.50 ± 0.25 ns and 5.56 ± 0.14 ns at 600 and 500 MHz, respectively. These correlation times were determined as averages from per residue fits of the relaxation data to the $S^2 - \tau_m$ model excluding residues with $NOE^{600} < 0.65$ and $NOE^{500} < 0.60$ (Farrow et al., 1994). The agreement between 500 and 600 MHz data is good, and the correlation time confirms that recombinant eotaxin is in the monomeric state. For comparison, the τ_m of the monomeric CX_3C chemokine fractalkine is 6.0 ns (Mizoue et al., 1999), monomeric vMIPII is 4.7 ns (LiWang et al., 1999), monomeric MIP(9) (analog of MIP-1β) is 4.5 ns while MIP-1β dimer is 8.6 ns (Laurence et al., 1998).

For eotaxin the $D_{\|}/D_{\perp}$ ratio was estimated at 0.87 (oblate) at 600 MHz and 0.94 at 500 MHz for an axially symmetric anisotropic diffusion tensor. Although the orientation of the principal axis of the rotational diffusion tensor is similar for the 600 and 500 MHz data, there is a discrepancy in the degree of anisotropy. In fact, the fit of the 500 MHz data was poor, and the probability that it occurred by chance was greater than 50%. The 600 MHz data were fit well by the axially symmetric diffusion tensor, and this reveals a small but measurable anisotropy. The probability that the experimentally observed diffusion anisotropy is caused by random error in the data is 0.08. This value is relatively high when compared to other studies (Tjandra et al., 1995; Gagné et al., 1998) but inevitable since only a small portion (32) core residues in the β-strands and α-helix satisfied the criteria for inclusion in an anisotropic analysis. Surprisingly, vMIP-II has been reported to show a rotational diffusion anisotropy of $D_{\|}/D_{\perp} = 1.5$ (prolate), very different to eotaxin despite an extremely similar tertiary structure (LiWang et al., 1999). For vMIP-II the T_1/T_2 ratios were extremely uniform (approximately 3.0) over the core residues suitable for selection in the authors determination of anisotropy so it is unclear how such a value was achieved.

The rigid core of eotaxin

The core regions of secondary structure defined as strand β1 (Ser25 to Ile29), β2 (Ala38 to Lys43), β3 (Asp48 to Ala51), and the α-helix (residues 57 to 68) have the most rigid backbone on the nanosecond to picosecond timescale characterized by $S^2_{600} = 0.83 \pm 0.04$ and $S^2_{500} = 0.82 \pm 0.03$ (not including figures for Ala51 and Ala38, see Fig. 3C). The dynamics study identifies

these residues as the most ordered, which agrees well with previous structural studies. Figure 8 compares the backbone order parameters derived in this study with the backbone RMSD values obtained from the family of 32 NMR structures (Crump et al., 1998). Although no direct relation exists between S^2 and the RMSD, regions that lack definition in the NMR structures such as the N- and C-termini show the smallest S^2 while the regions with low RMSD show the highest S^2 values. However, the dynamics data do suggest that there are motions in the N-loop that are not as apparent from the RMSD plot. In this sense, the structural connectivities may not have been sensitive to the motions that are present in this region (a fluctuating distance between two protons will tend to bias the NOE to the closest distance) and as a result may be overconstrained along this stretch of residues.

Motions in the N-terminus

Order parameters for the N-terminus of eotaxin (Ala3–Arg8) vary between 0.26 and 0.70 (Fig. 8). Order parameters decrease steadily and measured T_1 and T_2 values increase as the N-terminus is approached. Negative NOE values and extensive motions on the picosecond timescale are indicative of a chain that becomes increasingly disordered as it extends out into solution. The N-terminus is constrained by the CC disulfide bridge but preceding this there are relatively few tertiary interactions with the core structure of the protein. It therefore is not surprising that we observe large amplitude motions for this region of the protein at our measurement temperature of 30 °C. In the monomeric fractalkine (Mizoue et al., 1999; study at 22.5 °C) and vMIP-II (LiWang et al., 1999; study at 25 °C), similar high amplitude motions occur, suggesting this may be a generally observed trend in monomeric chemokines.

Motions in the N-loop

The N-loop is defined here as including residues succeeding the CC motif up until the 3_{10} turn (11–19). Both Phe11 and Asn12 give extremely weak ^{15}N–^{1}H correlations and no data could be acquired for Phe11, even when specifically labeled in the N1 peptide. Asn12 fits an $S^2 - \tau_m - R_{ex}$ model at 500 and 600 MHz, and it is reasonable to speculate that Phe11 is undergoing a similar slow conformational exchange resulting in attenuated signal amplitude. The remainder of the N-loop has low S^2 values when compared to the "core" residues ($S^2_{500} = 0.72 \pm 0.05$, $S^2_{600} = 0.70 \pm 0.05$ vs. 0.82).

Residues that show conformational exchange (30s loop, Ala51, Thr8)

The relaxation data recorded at multiple fields strongly suggest the presence of a slow (micro to millisecond) conformational exchange within the 30s loop, Thr8, Asn12, and Ala51. The $R_{ex}^{600}/R_{ex}^{500}$ ratios observed are close to theoretical values and are strong evidence for conformational exchange.

Figure 9 shows a ribbon diagram with a width proportional to the amplitude of motion given by $1 - S^2$ and residues that show a slower timescale motion (millisecond) are shaded in purple. The 30s loop, Thr8, Asn12, and Ala51 form a distinct unit connected by the two disulfide bonds (Fig. 9). In the ensemble of NMR structures, the backbone angular order parameters of residues Thr8–Asn12 and residues in the 30s loop (for Thr30–Cys34) are significantly reduced. Conversely, Ala51 showed much higher angular order parameters ($\boldsymbol{S}(\phi) = 1.00$ and $\boldsymbol{S}(\psi) = 1.00$). The χ^2 angle of the first disulfide bond (9–34) is disordered in the NMR structure, and the second disulfide (10–50) adopts a single con-

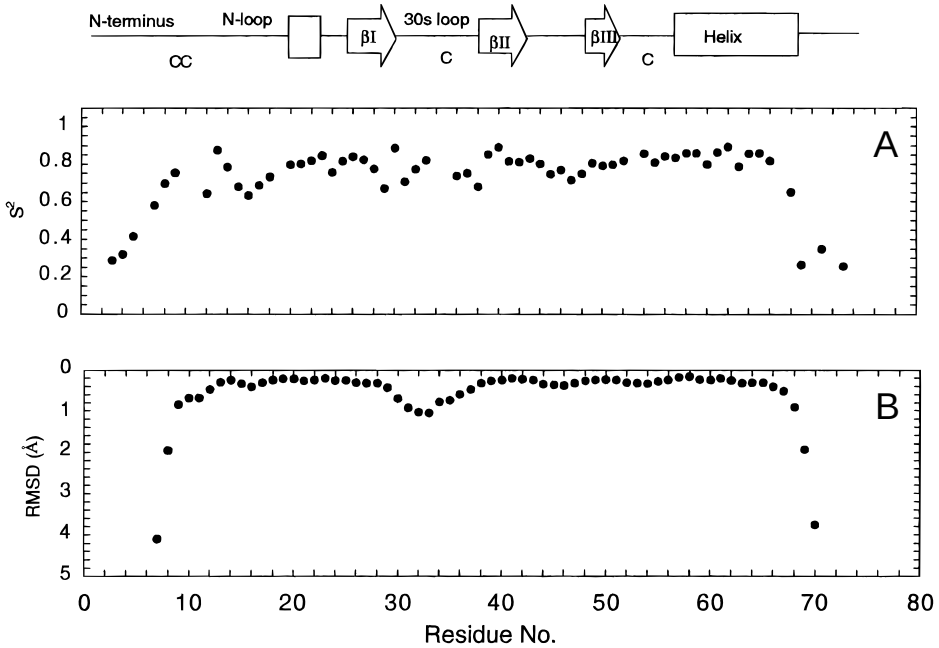

Fig. 8. Comparison between a structurally derived RMSD plot and backbone order parameters (S^2) derived from the present study. **A:** The backbone nitrogen order parameters (S^2) at 600 MHz. **B:** The backbone RMSD of the ensemble of NMR structures (Crump et al., 1998). The secondary structure elements are shown on the top of the figure.

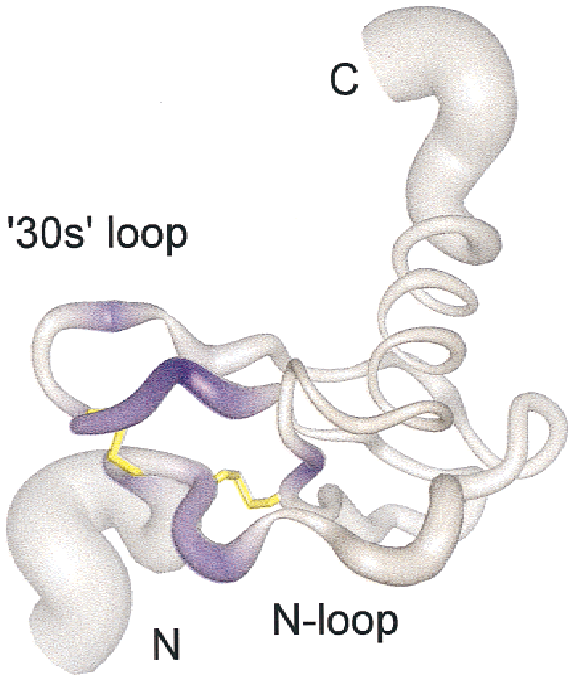

Fig. 9. Ribbon diagram of eotaxin where the ribbon thickness is proportional to the amplitude of fast internal motions $1 - S^2$. Residues that exhibit conformational exchange (significant R_{ex} terms) are shaded in purple with the depth of color proportional to the size of the R_{ex} term (600 MHz).

formation. In the case of the 30s loop and the residues surrounding the first disulfide, the slow motions may arise for several reasons. First, the residues are in general proximity to the rapid motions of the N-terminus, and second, there are relatively few tertiary interactions between the 30s loop and residues adjacent to the first disulfide. The first disulfide itself may be undergoing rapid conformational fluctuations that slowly modulate the separation between N-terminus and 30s loop resulting in a coupled slow motion. Ala51 and Ala38 display the largest R_{ex} terms at both 500 and 600 MHz, and while the positioning of Ala38 in the 30s loop makes this less surprising, Ala51 is more unusual as it is situated in the more rigid "core" of the protein. Ala38 is in close proximity to, but not in direct contact with, Ala51 but they are both in close proximity to the second disulfide bond. The amide bond of Ala51 points inward toward the disulfide linkage and the methyl group of Ala38 packs against the disulfide. Lacking other explanations of these motions, it is therefore possible that despite appearing structured in the NMR ensemble, the second disulfide may undergo conformational fluctuations or a slower isomerization that induces a slowly changing chemical environment for Ala38 and Ala51. Alternatively Ala38, Ala51, Asn12, and perhaps even Cys10 and Phe11 may all be undergoing slow motion induced by motion in the second disulfide. A similar dynamic equilibrium has been characterized in BPTI and shown to give rise to millisecond motions of residues adjacent to the disulfide bonds (Szyperski et al., 1993).

We have also attempted to characterize motions in the dimer structure by examining a synthetic sample of eotaxin. We have shown previously that eotaxin without an N-terminal extension is in exchange between monomer and dimer. For core residues that showed no chemical shift difference between the monomer and dimer, the T_1 and T_2 parameters were fitted to biexponential decays and showed values similar to core residues in the MIP-1β dimeric structure (Laurence et al., 1998). We were also able to obtain results for two residues that displayed microsecond to millisecond conformational exchange in the monomer, Ser31 and Ala51. Both show nitrogen and amide proton chemical shift changes upon dimerization suggesting a possible structural or dynamical change, but more surprising is the observation that after taking into account the monomer–dimer exchange, their fitted T_2 values are similar to that of other "core" like residues of the dimer. This would suggest that the millisecond timescale motions that are observed in the eotaxin monomer might be attenuated upon dimerization. This idea is not without merit as the dimer interface identified in other CC chemokines involves numerous intersubunit contacts between N-terminus, N-loop, 30s loop, and residues in β3. Previous NMR studies have also suggested that a similar dimer interface is formed for eotaxin (Crump et al., 1998). Quaternary interactions formed upon dimerization may lead to a stabilization of the complex and reduce the amplitudes of motions in the monomer subunit. A "tightening" of the structure of IL-8 has been suggested in a previous study that compared amide exchange rates of a monomeric IL-8 subunit with the corresponding dimer (Rajarathnam et al., 1994). We do exercise, however, some caution in the interpretation of only a limited sample of relaxation parameters, and this will be an area of future study.

Relationship of dynamics to structure/function of the chemokines

Numerous studies have addressed the functional role of chemokine oligomerization and structural determinants of receptor binding/activation or discrimination (Clark-Lewis et al., 1995 (and references therein); Baggiolini et al., 1997). The critical receptor binding regions are in the first 20 residues of both the CC and CXC chemokines. Often the N-terminus preceding the disulfide bonds is the most critical, controlling both receptor binding and activation while the N-loop succeeding the disulfides forms a second but somewhat less critical binding site. Additional sites have been identified by mutagenesis in different chemokines including residues within the first β-strand (edge) and the 30s loop. The well-structured regions of the protein are not directly implicated in receptor binding, and we have previously proposed that they provide a scaffold that presents the receptor with the binding regions in an optimal fashion (Clark-Lewis et al., 1994). Recent structural studies have begun to confirm this hypothesis through examination of chemokine structure/function and even complexes of chemokines and receptor fragments. In particular, IL-8 and a CXCR-1 based peptide are found to interact along the N-loop of IL-8, a binding region thought to control specificity for CXCR-1 over CXCR-2 (Skelton et al., 1999).

This study and other backbone ^{15}N relaxation studies on the IL-8 dimer and monomeric chemokines reveal flexible N-termini (Grasberger et al., 1993; LiWang et al., 1999; Mizoue et al., 1999). Conversely the N-terminus in the CC chemokine dimer appears to be well structured in several structural NMR studies (Fairbrother & Skelton, 1996). It has been speculated that the differing dimer structures and properties of CXC and CC may dictate CXCR and CCR specificity or furthermore be a fundamental requirement for chemokine activity (Baggiolini et al., 1997 and references therein). On the other hand, engineered monomeric chemokines do remain active (Rajarathnam et al., 1994) and MCP-1 has been shown to

dimerize in both forms (Lubkowski et al., 1997). Regardless of the arguments for and against, if the monomeric form is the active chemokine species then the physiological relevance of flexibility in the N-terminus must be addressed. On the one hand, the N-terminus is free to explore multiple conformations in solution, including the "bound" state. Similarly, the slow motions in the 30s loop, N-loop, and perhaps the disulfide bond(s) may allow this region to exchange between two or more states, again including a "bound" form. The question is can we reconcile these motions with a picture other than the normal "static" complex? If we first make the assumption that the structure of the extracellular receptor loops are not static and that the amplitude of the fluctuations are of similar magnitude to the ligand, then the answer might reside in the fact that the structure of the free chemokine is undergoing conformational fluctuations to match a fluctuating receptor. In the broader sense, this could be an advantage for affinity and molecular recognition. The molecular recognition may benefit from the fact that the probability of a fluctuating receptor being recognized by a ligand should be higher when the ligand itself is fluctuating. In other words, it could be a kinetic advantage to have a ligand and receptor that are able to sample many potentially competent "bound" forms. Then assuming a complex that also fluctuates (as opposed to a static complex), the stability of the complex may benefit from a "dynamic" close packing that maintains the favorable enthalpic contributions one associates with a "static" complex, while reducing the unfavorable loss of conformational and vibrational entropy. The precise nature of the interaction is difficult to predict, except to say that it is likely that entropic considerations may fine tune the free energy of binding (affinity). Some answers may come from looking at changes in order parameters between the free state and the bound state of the chemokine. This would allow changes in conformational entropy to be estimated (Yang & Kay, 1996), and we are currently pursuing these goals in our laboratory. Ultimately chemokine binding must be strong enough to maintain agonist driven desensitization of the receptor but not prevent the eventual resensitization.

Materials and methods

Sample preparation

Recombinant human eotaxin was prepared from the eotaxin gene subcloned into an expression vector pET15b (Novagen, Madison, Wisconsin) in *Escherichia coli* strain BL21(DE3) as previously described (Crump et al., 1998). Two synthetic eotaxin samples with specifically backbone ^{15}N labeled sites were synthesized by stepwise solid phase methods using t-Boc protection chemistry. Peptide 1, termed N1, was labeled with Phe11, Ser31, and Gly32. Peptide 2, termed N2, was labeled with Leu20, Leu23, Val39, Ala51, Val58, and Ser61. After hydrogen fluoride deprotection, the polypeptides were folded and purified as described previously (Clark-Lewis et al., 1994). Purity of the products was assessed by ion-exchange HPLC and mass spectrometry. The measured mass of each of the final products, as determined by electrospray mass spectrometry, was consistent with the average mass calculated from the atomic composition.

NMR samples (1 mM) were prepared by dissolving the lyophilized protein in 500 μL of sodium acetate buffer (90% ^1H_2O/10% ^2H_2O) containing 1 mM NaN_3 (sodium azide) and 1 mM DSS (2,2 dimethyl-silapentane-5-sulfonic acid). The pH was adjusted to 5.00 ± 0.10 (glass electrode, uncorrected for isotope effects) with NaO^2H.

NMR spectroscopy

NMR experiments were performed on Varian Unity 600 MHz and Varian Inova 500 MHz spectrometers equipped with *z*-axis pulsed field gradient triple resonance probes and a Varian Unity 300 MHz spectrometer with a 5 mm inverse detection probe (nonpulsed field gradient). ^{15}N-T_1, T_2, and $\{^1H\}$-^{15}N NOE experiments were conducted at 500 and 600 MHz using pulsed field gradient sequences previously described (Farrow et al., 1994). In these cases, pulsed field gradients were employed for coherence selection, sensitivity enhancement, and reduction of spectral artifacts. ^{1}H 180° pulses were used for elimination of cross-correlation effects between ^{1}H–^{15}N dipolar and ^{15}N CSA relaxation mechanisms during relaxation periods (Goldman, 1984; Kay et al., 1992). For the T_1 experiments, 550 μs cosine modulated rectangular pulses were employed with excitation maxima 2 kHz away from the carrier to minimally disturb the water resonance (Smallcombe, 1993; Farrow et al., 1994). At 300 MHz sensitivity-enhanced nongradient pulse sequences were adapted from those of Kördel (Kördel et al., 1992) and programmed in house. At 500 and 600 MHz, T_1 data were acquired using relaxation delays of 11.1, 55.5, 122.1, 199.8, 277.5, 388.5, 499.5, 666.0, 888.0, and 1,110 ms and at 300 MHz with delays of 10.0, 50.2, 100.3, 150.5, 200.6, 280.9, 361.2, 501.6, and 702.2 ms. T_2 data were acquired at 600 MHz using delays of 16.3, 32.6, 48.9, 65.2, 81.4, 97.7, 114.0, 130.3, 146.4, 162.88, and 179.17 ms, at 500 MHz with delays of 16.6, 33.3, 49.8, 66.5, 83.0, 99.7, 116.3, 132.9, 149.5, 166.1, and 182.7 ms and at 300 MHz with delays of 16.6, 33.2, 49.7, 66.3, 82.9, 99.5, 116.1, and 132.6 ms. For the T_2 pulse sequence, the delay between transients was 2.5 s at 500 and 600 MHz and 2.0 s at 300 MHz, and the field strengths for nitrogen decoupling and hard pulses are shown in Table 3. Keeping nitrogen powers to a minimum (3.7 to 4.2 kHz) coupled with sufficient delays between transients has been shown to drastically reduce the effects of sample heating (Gagné et al., 1998). $\{^1H\}$-^{15}N NOEs were measured by recording HSQC spectra with and without proton saturation (the field strengths for proton and nitrogen pulses and decoupling are shown in Table 2). The spectra recorded at all three fields without NOE were recorded with delays of 5 s and spectra with NOE used 3 s of proton saturation and 2 s of delay to give the same total delay of 5 s between transients.

Data processing

All spectra were processed with the program NMRPipe (Delaglio et al., 1995). Ninety-degree-shifted sine and sine-squared window functions were applied in t_2 and t_1, respectively, and both dimensions were baseline corrected using the *POLY*-auto function. Linear prediction was used to extend the experimental points in the t_1 dimensions by 25 or 50%, and t_1 and t_2 dimensions were zero filled to twice the number of points. The first two-dimensional spectrum of a 300, 500, and 600 MHz ^{15}N T_1 or T_2 series was peak picked manually using the program PIPP (Garrett et al., 1991). Subsequent spectra in a series were automatically picked using the program CAPP (Garrett et al., 1991) allowing the whole procedure to be automated. T_1 and T_2 values were obtained by nonlinear least-squares fits of the amide cross-peak intensities to a two-parameter exponential decay using software provided by Lewis E. Kay. Uncertainties in the T_1 and T_2 values were estimated from the

Table 3. *Acquisition parameters for eotaxin ^{15}N relaxation at 300, 500, and 600 MHz*

Experiment Field (MHz)	^{15}N-T_1 600	^{15}N-T_1 500	^{15}N-T_1 300	^{15}N-T_2 600	^{15}N-T_2 500	^{15}N-T_2 300	{^{1}H}^{15}N NOE 600	{^{1}H}^{15}N NOE 500	{^{1}H}^{15}NOE 300
γB_1 (kHz)									
^{1}H pulses	28	29	31	28	29	31	28	29	31
^{1}H saturation							11.4[a]	10	14
^{15}N pulses	5.3	6.5	3.7	4.2	3.6	3.7	5.3	6.5	3.7
^{15}N dec. (WALTZ)	0.8	1.1	0.6	0.8	1.1	0.6	0.8	1.1	0.6
^{15}N (CPMG)							4.2	3.6	3.7
F_2 sw[b] (kHz)	8.0	7.0	4.0	8.0	7.0	4.0	8.0	7.0	4.0
F_1 sw[b] (kHz)	1.6	1.3	0.7	1.6	1.3	0.7	1.6	1.3	0.7
F_2 points[c]	512	512	320	512	448	320	512	512	320
F_1 points[c]	128	64	48	128	96	40	128	64	48
Transients	8	48	128	8	32	256	32	160	96

[a] Sat indicates a saturation pulse train with 120° pulses applied every 5 ms.
[b] Spectra width.
[c] Real points.

nonlinear least-squares fits. Uncertainties in the NOE values were estimated from the baseplane noise in two-dimensional {^{1}H–^{15}N}-HSQC spectra recorded with and without proton saturation according to Farrow et al. (1994).

Theory

The theoretical basis for T_1, T_2, and NOE relaxation of ^{15}N is well established. These quantities are related to a spectral density function at ^{1}H and ^{15}N frequency combinations (ω) (Abragam, 1961). It is popular to relate these data to motional parameters using the "model free" assumption for the correlation function (Lipari & Szabo, 1982a, 1982b) where the spectral density function is

$$J(\omega) = 2/5((S^2\tau_m/(1 + (\omega\tau_m)^2) + (1 - S^2)\tau/(1 + (\omega\tau)^2)) \quad (8)$$

where τ_m is the overall correlation time (isotropic tumbling is assumed), S^2 is the order parameter, $\tau^{-1} = \tau_m^{-1} + \tau_e^{-1}$, and τ_e is the effective correlation time describing fast internal motions. These are referred to as $S^2 - \tau_m$ or $S^2 - \tau_m - \tau_e$ models, depending on whether a fast motion is required for the fit or not. Model free parameters from the experimental data were obtained by minimizing a target function (Equation 9) describing the differences between experimental relaxation parameters and relaxation parameters calculated from the spectral density functions assumed,

$$\chi^2 = \left[\frac{T_1^e - T_1^c}{\sigma T_1}\right]^2 + \left[\frac{T_2^e - T_2^c}{\sigma T_2}\right]^2 + \left[\frac{\mathrm{NOE}^e - \mathrm{NOE}^c}{\sigma \mathrm{NOE}}\right]^2 \quad (9)$$

where the superscripts e and c denote experimental data and calculated values, respectively; σ is the experimental error associated with the measurement; and χ^2 is the squared sum of the residual errors for all nuclei n. χ^2 is minimized for residues individually except when a "global" optimum τ_m is calculated.

In cases where the relaxation data did not fit an $S^2 - \tau_m$ or $S^2 - \tau_m - \tau_e$ model, an additional model was considered that incorporates conformational exchange as an R_{ex} term in the T_2 equations:

$$1/T_2 = 1/T_{2(DD)} + 1/T_{2(CSA)} + R_{ex} \quad (10)$$

where $T_{2(DD)}$ and $T_{2(CSA)}$ represent the ^{1}H–^{15}N dipole-dipole and ^{15}N chemical shift anisotropy contributions to the measured T_2. These models are referred to as $S^2 - \tau_m - R_{ex}$ or $S^2 - \tau_m - \tau_e - R_{ex}$. In addition, internal motions were accounted for with a two-timescale model (Clore et al., 1990a, 1990b) that allows internal motions to occur on two distinct timescales. This leads to the following expression for the spectral density, referred to as a two-timescale model:

$$J(\omega) = 2/5((S^2\tau_m/(1 + (\omega\tau_m)^2) + (S_f^2 - S^2)\tau/(1 + (\omega\tau)^2)) \quad (11)$$

where $S^2 = S_f^2 S_S^2$ and $1/\tau = 1/\tau_m + 1/\tau_s$. S_f^2 and S_s^f are the order parameters characterizing the fast (picosecond) and slow (nanosecond) motions, respectively, and τ_s is the effective correlation time for the slow internal motions. Equation 11 omits an additional term for fast internal motions that have been shown to contribute negligibly to the relaxation (Clore et al., 1990b). Analysis of data with an anisotropic tumbling model was also considered as reported by Tjandra et al. (1995).

Acknowledgments

We acknowledge Gerry McQuaid for maintenance of the spectrometers and Lewis E. Kay for pulse sequences. We would also like to acknowledge Stéphane Gagné for several useful UNIX scripts. This work was supported by the Protein Engineering Network of Centres of Excellence (PENCE) and a grant from the Korean Ministry of Health and Welfare to K.-S.K.

References

Abragam A. 1961. *Principles of nuclear magnetism*. Oxford, UK: Clarendon Press.

Baggiolini M, Dewald B, Moser B. 1997. Human chemokines: An update. *Annu Rev Immunol 15*:675–705.

Bevington PR, Robinson DK. 1992. *Data reduction and error analysis for the physical sciences*, 2nd ed. New York: McGraw-Hill.

Clark-Lewis I, Dewald B, Loetscher M, Moser B, Baggiolini M. 1994. Structural requirements for interleukin-8 function identified by design of analogs and CXC chemokine hybrids. *J Biol Chem 269*:16075–16081.

Clark-Lewis I, Kim KS, Rajarathnam K, Gong J-H, Dewald B, Moser B, Baggiolini M, Sykes BD. 1995. Structure-activity relationships of chemokines. *J Leukocyte Biol 57*:703–711.

Clore GM, Driscoll PC, Wingfield PT, Gronenborn AM. 1990a. Analysis of the backbone dynamics of interleukin-1 beta using two-dimensional inverse detected heteronuclear ^{15}N-^{1}H NMR spectroscopy. *Biochemistry 29*:7387–7401.

Clore GM, Szabo A, Bax A, Kay LE, Driscoll PC, Gronenborn AM. 1990b. Deviations from the simple two-parameter model-free approach to the interpretation of nitrogen-15 nuclear magnetic relaxation of proteins. *J Am Chem Soc 112*:4989–4991.

Corrigan CJ, Kay AB. 1992. T-cells and eosinophils in the pathogenesis of asthma. *Immunol Today 13*:501–507.

Crump MP, Gong J-H, Loetscher P, Rajarathnam K, Amara A, Arezana-Seisedos F, Virelizier J-L, Baggiolini M, Sykes BD, Clark-Lewis I. 1997. Solution structure and basis for functional activity of stromal cell-derived factor-1; dissociation of CXCR4 activation from binding and inhibition of HIV-1. *EMBO J 16*:6996–7007.

Crump MP, Rajarathnam K, Kim K-S, Clark-Lewis I, Sykes BD. 1998. Solution structure of eotaxin, a chemokine that selectively recruits eosinophils in allergic inflammation. *J Biol Chem 273*:22471–22479.

Delaglio F, Grzesiek S, Vuister GW, Zhu G, Pfeifer J, Bax A. 1995. NMRpipe: A multidimensional spectral processing system based on UNIX pipes. *J Biomol NMR 6*:277–293.

Fairbrother WJ, Skelton NJ. 1996. Three dimensional structures of the chemokine family. In Horuk R, ed. *Chemoattractant ligands and their receptors*. London, UK: CRC Press. pp 55–86.

Farrow NA, Muhandiram R, Singer AU, Pascal SM, Kay CM, Gish G, Shoelson SE, Pawson T, Forman-Kay JD, Kay LE. 1994. Backbone dynamics of a free and a phosphopeptide-complexed Src homology 2 domain studied by ^{15}N-relaxation. *Biochemistry 33*:5984–6003.

Farrow NA, Zhang O, Forman-Kay JD, Kay LE. 1995. Comparison of the backbone dynamics of a folded and an unfolded SH3 domain existing in equilibrium in aqueous buffer. *Biochemistry 34*:868–878.

Gagné SM, Tsuda S, Spyracopoulos L, Kay LE, Sykes BD. 1998. Backbone and methyl dynamics of the regulatory domain of troponin C: Anisotropic rotational diffusion and contribution of conformational entropy to calcium affinity. *J Mol Biol 278*:667–686.

Garrett DS, Powers R, Gronenborn AM, Clore GM. 1991. A common sense approach to peak picking in two-, three, and four-dimensional spectra using automatic computer analysis of contour diagrams. *J Magn Reson 95*:214–220.

Goldman M. 1984. Interference effects in the relaxation of a pair of unlike spin one-half nuclei. *J Magn Reson 60*:437–452.

Gong J-H, Uguccioni M, Dewald B, Baggiolini M, Clark-Lewis I. 1996. RANTES and MCP-3 antagonists bind multiple chemokine receptors. *J Biol Chem 271*:10521–10527.

Grasberger BL, Gronenborn AM, Clore GM. 1993. Analysis of the backbone dynamics of interleukin-8 by ^{15}N relaxation measurements. *J Mol Biol 230*:364–372.

Griffiths-Johnson DA, Collins PD, Rossi AG, Jose PJ, Williams TJ. 1993. The chemokine, eotaxin, activates guinea-pig eosinophils in vitro and causes their accumulation in the lung in vivo. *Biochem Biophys Res Commun 197*:1167–1172.

Hyberts SG, Goldberg MS, Havel TF, Wagner G. 1992. The solution structure of eglin c based on measurements of many NOEs and coupling constants and its comparison to the X-ray structure. *Protein Sci 1*:736–751.

Jeener J, Meier BH, Bachmann P, Ernst RR. 1979. Investigation of exchange processes by two-dimensional NMR spectroscopy. *J Chem Phys 71*:4546–4553.

Jose PJ, Griffiths-Johnson DA, Collins PD, Walsh DT, Moqbel R, Totty NF, Truong O, Hsuan JJ. 1994. Eotaxin: A potent eosinophil chemoattractant cytokine detected in a guinea pig model of allergic airways inflammation. *J Exp Med 179*:881–887.

Katoh E, Yamazaki T, Kiso Y, Wingfield PT, Stahl SJ, Kaufman JD, Torchia DA. 1999. Determination of the rate of monomer interchange in a ligand bound homodimeric protein from NOESY crosspeaks: Application to HIV protease/KNI-529 complex. *J Am Chem Soc 121*:2607–2608.

Kay LE, Nicholoson LK, Delaglio F, Bax A, Torchia DA. 1992. Pulse sequences for removal of the effects of cross-correlation between dipolar and chemical-shift anisotropy relaxation mechanisms on the measurement of heteronuclear T_1 and T_2 values in proteins. *J Magn Reson 97*:359–375.

Kay LE, Torchia DA, Bax A. 1989. Backbone dynamics of proteins as studied by ^{15}N inverse detected heteronuclear NMR spectroscopy: Application to staphylococcal nuclease. *Biochemistry 28*:8972–8979.

Kim K-S, Rajarathnam K, Clark-Lewis I, Sykes BD. 1996. Structural characterization of a monomeric chemokine: Monocyte chemoattractant protein-3. *FEBS Lett 395*:277–282.

Kitaura M, Nakajima T, Imai T, Harada S, Combadiere C, Lee Tiffany H, Murphy PM, Yoshie O. 1996. Molecular cloning of human eotaxin, an eosinophil-selective CC chemokine, and identification of a specific eosinophil eotaxin receptor, CC chemokine receptor 3. *J Biol Chem 271*:7725–7730.

Kördel J, Skelton NJ, Akke M, Palmer AG, Chazin WJ. 1992. Backbone dynamics of calcium-loaded calbindin D_{9k} studied by two-dimensional proton-detected ^{15}N NMR spectroscopy. *Biochemistry 31*:4856–4866.

Laurence JS, LiWang AC, LiWang PJ. 1998. Effect of N-terminal truncation and solution conditions on chemokine dimer stability: Nuclear resonance structural analysis of macrophage inflammatory protein-1β mutants. *Biochemistry 37*:9346–9354.

Lipari G, Szabo A. 1982a. A model-free approach to the interpretation of nuclear magnetic resonance relaxation in macromolecules I. Theory and range of validity. *J Am Chem Soc 104*:4545–4549.

Lipari G, Szabo A. 1982b. A model-free approach to the interpretation of nuclear magnetic resonance relaxation in macromolecules II. Theory and range of validity. *J Am Chem Soc 104*:4549–4570.

LiWang AC, Cao JJ, Zheng H, Lu Z, Peiper SC, LiWang PJ. 1999. Dynamics study on the anti-human immunodeficiency virus chemokine viral macrophage-inflammatory Protein-II (vMIP-II) reveals a fully monomeric protein. *Biochemistry 38*:442–453.

Lowman HB, Slagle PH, DeForge LE, Wirth CM, Gillece-Castro BL, Bourell JH, Fairbrother WJ. 1996. Exchanging interleukin-8 and melanoma growth-stimulating activity receptor binding specificities. *J Biol Chem 271*:14344–14352.

Lubkowski J, Bujacz G, Boqué L, Domaille PJ, Handel TM, Wlodawer A. 1997. The structure of MCP-1 in two crystal forms provides a rare example of variable quaternary structures. *Nat Struct Biol 4*:64–69.

McConnell HM. 1958. Reaction rates by nuclear magnetic resonance. *J Chem Phys 28*:430–431.

Mizoue LS, Bazan JF, Johnson EC, Handel TM. 1999. Solution structure and dynamics of the CX_3C chemokine domain of fractalkine and its interaction with an N-terminal fragment of CX_3CR1. *Biochemistry 38*:1402–1414.

Pakianathan DR, Kuta EG, Artis DR, Skelton NJ, Hébert CA. 1997. Distinct but overlapping epitopes for the interaction of a CC-chemokine with CCR1, CCR3, and CCR5. *Biochemistry 36*:9642–9648.

Palmer AG. 1993. Dynamic properties of proteins using NMR spectroscopy. *Curr Opin Biotechnol 4*:385–391.

Ponath PD, Qin S, Ringler DJ, Clark-Lewis I, Wang J, Kassam N, Smith H, Shi X, Gonzalo J-A, Newman W, et al. 1996. Cloning of the human eosinophil chemoattractant, eotaxin. *J Clin Invest 97*:604–612.

Rajarathnam K, Sykes BD, Dewald B, Baggiolini M, Clark-Lewis I. 1999. Disulfide bridges in interleukin-8 probed using non-natural disulfide analogues: Dissociation of roles in structure from function. *Biochemistry 38*:7653–7658.

Rajarathnam K, Sykes BD, Kay CM, Geiser T, Dewald B, Baggiolini M, Clark-Lewis I. 1994. Neutrophil activation by monomeric interleukin-8. *Science 264*:90–92.

Sallusto F, Mackay CR, Lanzavecchia A. 1997. Selective expression of the eotaxin receptor CCR3 by human T helper 2 cells. *Science 277*:2005–2007.

Schraufstätter IU, Ma M, Oades ZG, Barritt DS, Cochrane CG. 1995. The role of Tyr13 and Lys15 of interleukin-8 in the high affinity interaction with the interleukin-8 receptor type A. *J Biol Chem 270*:10428–10431.

Skelton NJ, Quan C, Reilly D, Lowman H. 1999. Structure of a complex between interleukin-8 and a CXCR-1 receptor based peptide. *Structure 7*:157–168.

Smallcombe SH. 1993. Solvent suppression with symmetrically shifted pulses. *J Am Chem Soc 115*:4776–4785.

Szyperski T, Luginbühl P, Otting G, Wüthrich K. 1993. Protein dynamics studied by rotating frame 15N spin relaxation times. *J Biomol NMR 3*:151–164.

Tjandra N, Feller SE, Pastor RW, Bax A. 1995. Rotational diffusion anisotropy of human ubiquitin from ^{15}N NMR relaxation. *J Am Chem Soc 117*:12562–12566.

Tjandra N, Wingfield P, Stahl S, Bax A. 1996. Anisotropic rotational diffusion of perdeuterated HIV protease from ^{15}N NMR relaxation measurements at two magnetic fields. *J Biomol NMR 8*:273–284.

Wagner G. 1993. NMR relaxation and protein mobility. *Curr Opin Struct Biol 3*:748–753.

Yang D, Kay LE. 1996. Contributions to conformational entropy arising from bond vector fluctuations measured from NMR-derived order parameters: Application to protein folding. *J Mol Biol 263*:369–382.